RSC Advances

ROYAL SOCIETY OF CHEMISTRY

www.rsc.org/advances

RSC Advances

ARTICLE

Directly ultrasonic modification of current collector with enhanced pseudocapacity

Received 00th January 20xx,
Accepted 00th January 20xx

DOI: 10.1039/x0xx00000x

www.rsc.org/

Zijun Shi[a], Qingwen Zhou[a], Yang Liu[a], Yanfang Gao[a,*] and Jinrong Liu[a]

In this work, we using directly ultrasonic modify nickel foam in the sulfuric acid, which achieve a simple and rapid binder-free electrode, improving the electronic transmission in the electrolyte. It make a bed of electroactive nickel hydroxide and sulphide with a unique needle-like microstructure , which grown vertically on the surface of the Ni foam straight into the electrolyte, not only increasing the contact interface area between the active material and the electrolyte but also shortening the diffusion length of the ions. The obtained product possesses outstanding electrochemical performance, having high specific capacitances of 6 F cm^{-2} at a current density of 5 mA cm^{-2}, which can still retain 2.2 F cm^{-2}, even at a current density as high as 40 mA cm^{-2} . Furthermore, it has excellent cyclic stability only 5% loss after 1000 cycles.

1. Introduction

Binder-free electrode is a very important class of porous electrode, which simplify preparation technique and effectively promote electronic with ionic transport properties [1]. The formation processes always is the active materials grow on the current collectors directly by chemical methods (e.g., hydrothermal growth, chemical vapour deposition, atomic layer deposition, and electroplating). By contrast, the conventional binder electrode is the poor electronic conductivity of the active material and can't be effectively compensated for by the tight integration of grow product on the current collector. For this reason, this design can neglect other auxiliary components of the configuration, such as conductive agents and binders, which are completely unnecessary in porous electrodes [2]. It is effective reduce the ionic diffusion resistance and improve more surface of active materials will be exposed and soaked. Although, it has been only a few years since this new concept come out, binder-free electrodes are being increasingly used in many types of energy storage devices, especially supercapacitors.

Various metals, such as Al, Cu, Ni, and stainless steel, are used as current collectors with binder-free electrodes in the form of thin foils, meshes or foams. Among these, nickel foam has attracted great interest as a current collector in supercapacitors, due to its high corrosion resistance and three-dimensional structure, which provides a larger surface area and better active material/electrolyte contact. To date, both electric double layer capacitive materials [3] (*e.g.*, graphene and carbon nanotubes) and pseudocapacitive materials [4] (*e.g.*, Co_3O_4, MnO_2, and $ZnCo_2O_4$) have been successfully grown on nickel foam used as capacitor electrodes. Based on the reversible conversion of nickel oxidation states from bivalent to trivalent. Nickel-containing compounds ($Ni(OH)_2$, Ni_3S_2, NiO, Ni_2P, $NiCl_2$, NiF_2, *etc.*) have become one of the most significant categories for using as active materials in binder-free pseudocapacitor electrodes. Furthermore, the substantial deposits and affordable cost also make nickel-based active materials become a promising candidate for commercial applications. One question that has been asked: what happened to the pseudocapacitive properties of binder-free electrodes when an in-situ modification on the current collectors? A more direct example of this broad question: can nickel elements from a nickel foam be transformed into nickel-containing compounds directly? Wang *et al.* reported on a self-supported binder-free Ni/NiO electrode configuration constructed via a nickel foam-based pyrogenic oxidation process where the porous core-shell structured Ni/NiO delivered improved performance as an anode for a lithium ion battery [5]. Analogously, Tang *et al.* proposed a simple two-step modification to activated carbon cloth, by wet chemical and thermal reduction treatments. The results of the modified that excellent wettability and a high surface area, which greatly enhanced its capacitive performance [6].

In this paper, a fast, practical and low cost electrode fabrication process is described. Nickel foam, used as the current collector, demonstrated a remarkably improved pseudocapacity via a simple ultrasonic modification in which a bed of electroactive nickel hydroxide and sulphide was formed on the surface of the foam directly through interfacial oxidation reactions. The enhanced electrochemical performance is primarily attributed to the surface formation of a unique needle-like microstructure, which minimized contact

[a] College of Chemical Engineering, Inner Mongolia University of Technology, Hohhot, 010051, P. R. China. Tel.: +86 471 6575722; Fax: +86 471 6503298
E-mail address: yf_gao@imut.edu.cn

†Electronic Supplementary Information (ESI) available: See DOI: 10.1039/x0xx00000x

resistance between the active materials and the Ni foam skeleton.

2. Experimental

2.1. Materials Synthesis

The Nickel foam (1 cm ×1 cm) was used as the current collector and cleaned with acetone and deionized water in an ultrasonic bath for 10 min. Subsequently, sonicated in a 6 M HCl solution for 20min and washed with deionized water and absolute ethanol. Then the water and ethanol on the surface of the Ni foam was soaked up with filter paper, the dried Ni foam was placed into 95.5 wt. % H_2SO_4 and subjected to ultrasonic processing for 5 min. The blackened Ni foam was soaked up with filter paper and placed into a 0.5 M KOH solution for another ultrasonic processing until no more floccule was generated on the surface. The obtained Ni foam was soaked up with filter paper and washed with deionized water and absolute ethanol three times. Finally, this modified Ni foam was soaked up once more with filter paper and used as the working electrode for electrochemical tests.

2.2. Materials Characterization

The as-prepared products were characterized with X-ray photo electron spectroscopy measurements (XPS; VG ESCALAB MARK II, Mg-Kα radiation), scanning electron microscopy (FESEM; JEOL, JSM-7600F), and transmission electron microscopy (TEM; JEOL, JEM-2100F) operated at 200 kV.

2.3. Electrochemical Measurements

Cyclic voltammetry (CV) and electrochemical impedance spectroscopy (EIS) measurements were performed using a potentiostat/galvanostat (Ametek, PAR 2273). EIS tests were performed in a frequency range of 0.01 to 10^5 Hz with an amplitude of 5 mV at the open circuit potential. The galvanostatic charge-discharge measurements were conducted on an electrochemical analyser (Chenhua, CHI 660E). All of the experiments were performed with a three-compartment cell in a 3 M KOH aqueous solution as the electrolyte. An Ag/AgCl electrode was used as the reference electrode, and a piece of platinum netting was employed as the counter electrode. To minimize any errors due to an *iR* drop in the electrolyte, the reference electrode was connected to the cell via a double salt bridge system and a Luggin capillary. After cell assembly, the working electrode was impregnated within the electrolyte for 2 h under vacuum to ensure that the electrode was thoroughly wetted. The specific capacitance (*C*) of the electrode was evaluated according to the following equation:

$$C = I \times \Delta t / \Delta V$$

where *C* (F cm^{-2}) is the specific capacitance of the electrode based on the area of electrode, *I* (mA cm^{-2}) is the current density during the discharge process, Δt (s) is the discharge time, and ΔV (V) is the potential window (here ΔV = 0.45 V).

3. Results and discussion

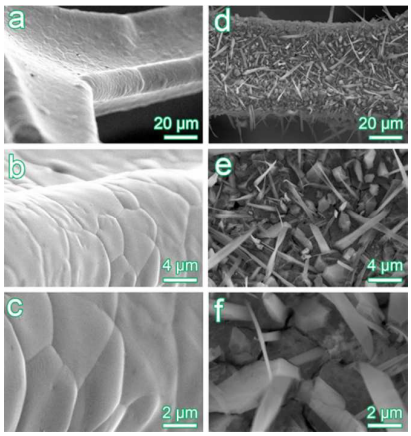

Fig.1. SEM images of the bare Ni foam and the modified nickel foam under different magnification. (a, b, c)The bare Ni foam; (d, e, f) The modified nickel foam.

The morphologies of the obtained electrodes were characterized using scanning electron microscopy (SEM), with the results shown in Fig. 1. Fig. 1a, b and c show the SEM images of the bare Ni foam, which exhibits a dense and smooth surface. These structural characteristics allow electrolyte easy access to the entire surface of the generated materials, which facilitates charge transport and ion diffusion without the limitations associated about the binder. After ultrasonic modification(Fig. 1d-f), the surface of the entire Ni foam becomes chapped and rough, as revealed in the spaces between the needle-like microstructure. In addition, observed that the nickel substrate is clearly covered by the previous inexistence of materials. Additionally, it was found that the materials had grown vertically on the entirety of the Ni foam to form a unique needle-like microstructure. The SEM images shown in Fig.S1† at

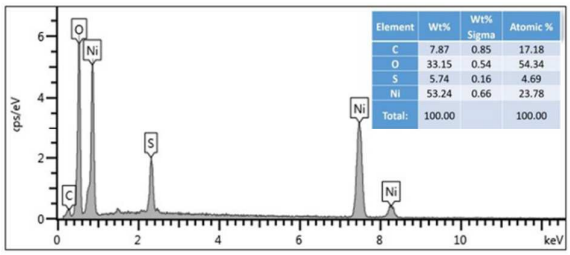

Fig. 2. EDS pattern of the target materials on the surface of Ni foam substrate.

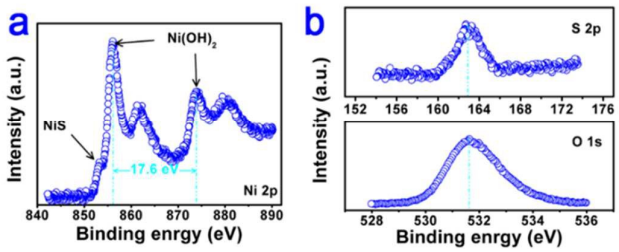

Fig. 3. The XPS spectra of the samples. (a) Ni 2p core; (b) O 1s and S 2p core.

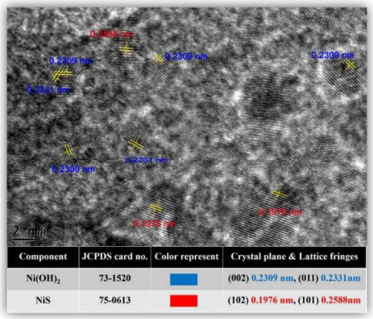

Fig.4. HRTEM images of the target materials on the surface of Ni foam substrate and analysis of the components based on the JCPDS Card No., Crystal plane and Lattice fringes.

other temperatures. Still keep the mesh structure at 5℃; at 30 ℃ exhibited flake-like; the result of Fig.S1c† shown globular structure, and with the increase of temperature, the reunion completely covered the surface of nickel foam.

Fig. 2 depicts the EDS pattern of generated materials on the surface of the Ni foam substrate and indicates the presence of Ni, O and S elements. The components of the generated materials are further verified by X-ray photoelectron spectroscopy (XPS) analysis. For the Ni 2p spectra (Fig. 3a), two Ni 2p core levels ($2p_{1/2}$ and $2p_{3/2}$) and two satellite peaks are observed. The binding energy of the Ni $2p_{3/2}$ peak is distinct from that be found in the literature for NiO (853.7 eV) and Ni (852.6 eV) [7, 8], but standardized to $Ni(OH)_2$ (856 eV) [9]. A spin-energy separation of 17.6 eV determined for $2p_{3/2}$ to $2p_{1/2}$ (873.5 eV) is also characteristic of the $Ni(OH)_2$ phase and is in good agreement with the literature [10]. Therefore, the results of this detailed analysis reveals that the components include $Ni(OH)_2$ and absent of NiO. In terms of literature, the binding energy of NiS is located at 853.1 eV [11] and S 2p core is found at 162.8 eV [12], simultaneously, $NiSO_4$ peak near 857.8 eV and S 2p core is found at 169.3 eV [12].

Through Fig. 3a and Fig. 3b we can know that the smaller shoulder peak near 853.1 (±0.2) eV and S 2p core is found at 162.8 eV. The search reveals that the components contains NiS instead of $NiSO_4$. The most likely source of the sulfide ion is the reduction of H_2SO_4 molecules [12].Furthermore, a more detailed verification of the formation of the electroactive nickel hydroxide and sulphide can be conducted with the help of high-resolution transmission electron microscopy (HRTEM). In Fig.4, Lattice fringes of 0.2309nm, 0.2331nm, 0.1976nm and 0.2588nm, respectively, according to JCPDS Card No., proved that the growth direction of the $Ni(OH)_2$ can be inferred as the crystal plane of (002) and (011), NiS can be inferred as the crystal plane of (102) and (101). Fig.S2† represented the N_2 adsorption and desorption isotherms of type IV accompanied by a H_3 hysteresis loop. And the pore size distribution curves at inset, which the main presence of mesoporous (4nm).

The electrochemical performances of the modified nickel foam when used as working electrodes for pseudocapacitors were investigated. The CV curves of the modified Ni foam

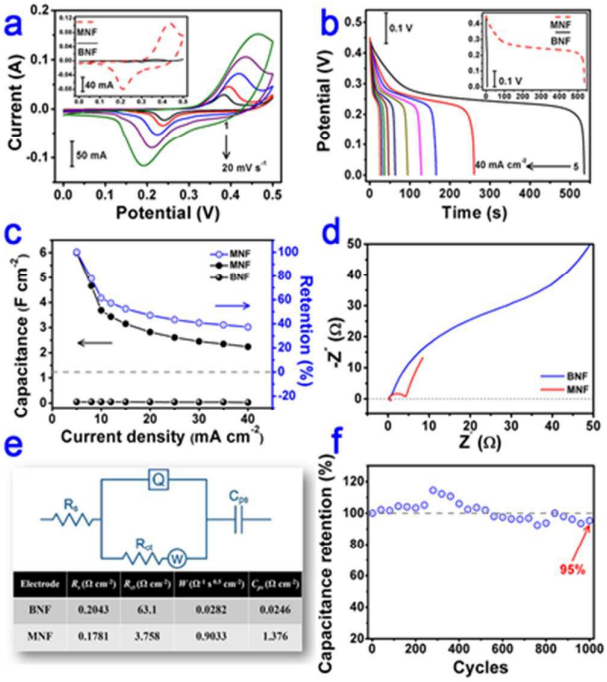

Fig. 5. Electrochemical characterization of the MNF and BNF electrodes. (a) CV curves of the MNF electrode at scan rates of 1, 2, 5, 10, and 20 mV s^{-1}; The inset shows the CV curves of the MNF and BNF at 10 mV s^{-1}; (b) Discharge curves of the MNF electrode at current densities of 5, 8, 10, 12, 15, 20, 25, 30, 35, and 40 mA cm^{-2}; The inset shows the discharge curve of the MNF and BNF at 10 mA cm^{-2}; (c) The corresponding specific capacitance (●) and capacity retention (○) as a function of different current densities; (d) Expanded views of the high frequency region of the Nyquist plots with the imaginary part (*Y*-axis) vs. the real part (*X*-axis) of the impedance from the EIS studies; (e) Electrical equivalent circuit used for fitting the impedance spectra and the calculated values of R_s, R_{ct}, W and C_{ps} determined via CNLS fitting of the experimental impedance spectra based on the equivalent circuit; (f) Cycling performance of the MNF electrode measured at a current density of 10 mA cm^{-2}.

(MNF) at different scan rates (1 to 20 mV s^{-1}) within the potential window of 0 to 0.45V in 3M KOH solution are shown in Fig. 5a. The redox peaks are maintained at different scan rates, and the shapes of these curves are similar, meaning the pseudocapacitive behaviour of the electrode is stable over this range. The anodic peak appeared indicates an oxidation process

due to the oxidation of $Ni(OH)_2$ to NiOOH and NiS to NiSOH, while the cathodic peak observed owing to the reverse process. The corresponding equation can be expressed as follows[10,13]:

$$Ni(OH)_2 + OH^- \leftrightarrow NiOOH + H_2O + e^-$$
$$NiS + OH^- \leftrightarrow NiSOH + e^-$$

The CV curves of the bare Ni foam (BNF) and the MNF measured at 10 mV s^{-1} are shown inset in Fig. 5a. The response current of the BNF is much weaker than that of the MNF, which illustrates the enhanced pseudocapacity that can be

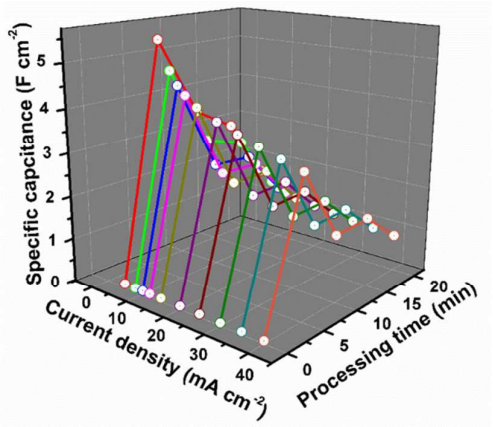

Fig.6. The corresponding specific capacitance as a function of different current densities for the modificatory Ni foams with different processing time.

obtained from the formation of electroactive nickel hydroxide and sulphide. The galvanostatic charge/discharge examination at 1 to 40 mA cm^{-2} is shown in Fig. 5b. The discharge range of the BNF at 10 mA cm^{-2} is negligible compared with the MNF (see the inset in Fig. 5b). The relationships between the specific capacitance or capacity retention and current density are illustrated in Fig. 5c. The specific capacitance can achieve a maximum of 6 F cm^{-2} at a current density of 5 mA cm^{-2}, which can still retain 2.2 F cm^{-2}, even at a current density as high as 40 mA cm^{-2}. For the BNF, the corresponding values at the same current densities are only 0.045 F cm^{-2} and 0.023 F cm^{-2}. This result numerically demonstrates that a fast ultrasonic modification for binder-free electrodes at ambient temperatures and pressures can result in a hundredfold or greater enhancement to the capacitance. In contrast with the other reported materials, the areal capacitance 1.62 F cm^{-2} at a discharge current density of 30 mA cm^{-2} for Ni@$Ni(OH)_2$ foams [14];Zhu acquired a specific capacitance of around 3.0 F cm^{-2} at a current density of 0.4 mA cm^{-2} for a NiO–TiO_2 electrode [15]. Additionally, electrodes with different processing times are also studied to determine the optimal fabrication parameters (Fig. 6). An ultrasonic modification period of 5 min was found to result in the best enhancement. The electrochemical impedance spectrum (EIS) was further carried out to investigate the electrochemical behaviour of the BNF and MNF electrodes. The corresponding Nyquist plots in a higher frequency area are shown in Fig. 5d. The measured impedance spectra were fitted using an equivalent circuit (Fig. 5e), which consisted of a bulk solution resistance R_s, charge-transfer resistance R_{ct}, constant phase angle element Q (or CPE), pseudocapacitive element C_{ps} from the redox process, and W (Warburg impedance). The inconspicuous MNF loop agrees with the smaller R_{ct} and may indicate a larger electroactive surface area [16]. Thus, more faradic reactions will occur and enhance the capacitance, which is shown by the value of C_{ps} (Fig. 5e). In addition, the long-term cyclic stability of the MNF electrodes was also investigated by repeating the galvanostatic charge/discharge tests at a very high current density of 10 mA cm^{-2} for ~1000 cycles, as shown in Fig. 5f. The specific capacitance increases gradually over the first ~300 cycles rather than decreases, which can be attributed to a complete activation of the modified electrodes [17]. More significantly, the decrease in the specific capacitance based on the initial value after 1000 cycles is only ~5%. The superior electrochemical performance of the MNF electrode mentioned.

Above is probably rooted in the following reasons. (i) The formation of nickel hydroxide and sulphide makes it possible for nickel elements in the Ni foam to take part in the faradic reactions. (ii) The one-dimensional needle-like microstructures grown vertically on the surface of the Ni foam gut straight into the electrolyte, not only increasing the contact interface area between the active material and the electrolyte but also shortening the diffusion length of the ions [18]. (iii) It is demonstrates how a binder-free electrode be composited by the in-situ transformation from metallic nickel to electroactive nickel-containing compounds, which provide for the high conductivity transport of electrons in the entire electrode and facilitate electrical activation.

4. Conclusions

In summary, a Nickel foam is modified via a fast and simple ultrasonic process at ambient temperatures and pressures. The generated active materials on the surface of the Ni substrate consisted of nickel hydroxide and sulphide, which exhibit a unique needle-like microstructure. During the examination of the capacitive performance of the product, the as-obtained electrodes demonstrate an ultra-high electrochemical activity (resulting in a hundredfold or more enhancement in the capacitance) and excellent cyclic stability (only ~5% loss after 1000 cycles) .The findings in this work demonstrate that an improved energy storage performance can be achievable quickly, practical and low cost fabrication methods.

Acknowledgements

This work was financially supported by the National Natural Science Foundation of China (No. 21266018), Science and technology projects of Science and Technology Department of Inner Mongolia Autonomous Region, P.R. China (No. 20110401 and No. 20130409), the Natural Science Foundation of Inner Mongolia, P.R. China (No. 2010MS0218), and the Program for Young Talents of Science and Technology in the Universities of Inner Mongolia Autonomous Region (No. NJYT-15-A04), the Ministry of Science and Technology China-South Africa Joint Research Program (No.CS08-L15) and the National Research Foundation (South Africa, CHN14033166025).

Notes and references

1 G. Q. Zhang, H. B. Wu, H. E. Hoster, M. B. Chan-Park and X. W. Lou, *Energy Environ. Sci.*, 2012, **5**, 9453.

2 J. Tian, Z. Xing, Q. Chu, Q. Liu, A. M. Asiri, A. H. Qusti, A. O. Al-Youbi and X. Sun, *CrystEngComm*, 2013, **15**, 8300.
3 Y. Zhai, Y. Dou, D. Zhao, P. F. Fulvio, R. T. Mayes and S. Dai, *Advanced materials*, 2011, **23**, 4828.
4 S. Liu, S. Sun and X.-Z. You, *Nanoscale*, 2014, **6**, 2037.
5 X. Li, A. Dhanabalan, K. Bechtold and C. Wang, *Electrochem. Commun.*, 2010, **12**, 1222.
6 S. Jiang, T. Shi, X. Zhan, H. Long, S. Xi, H. Hu and Z. Tang, *J. Power Sources*, 2014, **272**, 16.
7 G. S. Gund, D. P. Dubal, S. B. Jambure, S. S. Shinde and C. D. Lokhande, *J. Mater. Chem. A*, 2013, **1**, 4793.
8 M. C. Biesinger, B. P. Payne, L. W. M. Lau, A. Gerson and R. S. C. Smart, *Surf. Interface Anal.*, 2009, **41**, 324.
9 D. L. Legrand, H. W. Nesbitt and G. M. Bancroft, *Am. Mineral.*, 1998, **83**, 1256.
10 J. Yan, W. Sun, T. Wei, Q. Zhang, Z. Fan and F. Wei, *J. Mater. Chem.*, 2012, **22**, 11494.
11 H. W. Nesbitt, D. Legrand and G. M. Bancroft, *Phys. Chem. Miner.*, 2000, **27**, 357.
12 J. R. Kish, M. B. Ives and J. R. Rodda, *J. Electrochem. Soc.*, 2000, **147**, 3637.
13 C.C. Sun, M.Z. Ma, J. Yang, Y.F. Zhang, P. Chen, W. Huang and X.C. Dong, *Scientific reports*, 2014,**4**.
14 Q. Zhou, M. Cui, K. Tao, Y. Yang, X. Liu, L. Kang, *Applied Surface Science*, 2016,**365**, 125-130.
15 J. H. Kim, K. Zhu, Y. F. Yan, C. L. Perkins and A. J. Frank, *Nano Lett.*, 2010, **10**, 4099-104.
16 Q. Zhou, J. Xing, Y. Gao, X. Lv, Y. He, Z. Guo and Y. Li, *ACS Appl. Mater. Interfaces*, 2014, **6**, 11394.
17 H. Jiang, J. Ma and C. Li, *Chem. Commun.*, 2012, **48**, 4465.
18 X. Sun, C. Yan, Y. Chen, W. Si, J. Deng, S. Oswald, L. Liu and O. G. Schmidt, *Adv. Energy Mater.*, 2014, **4**, 1300912.

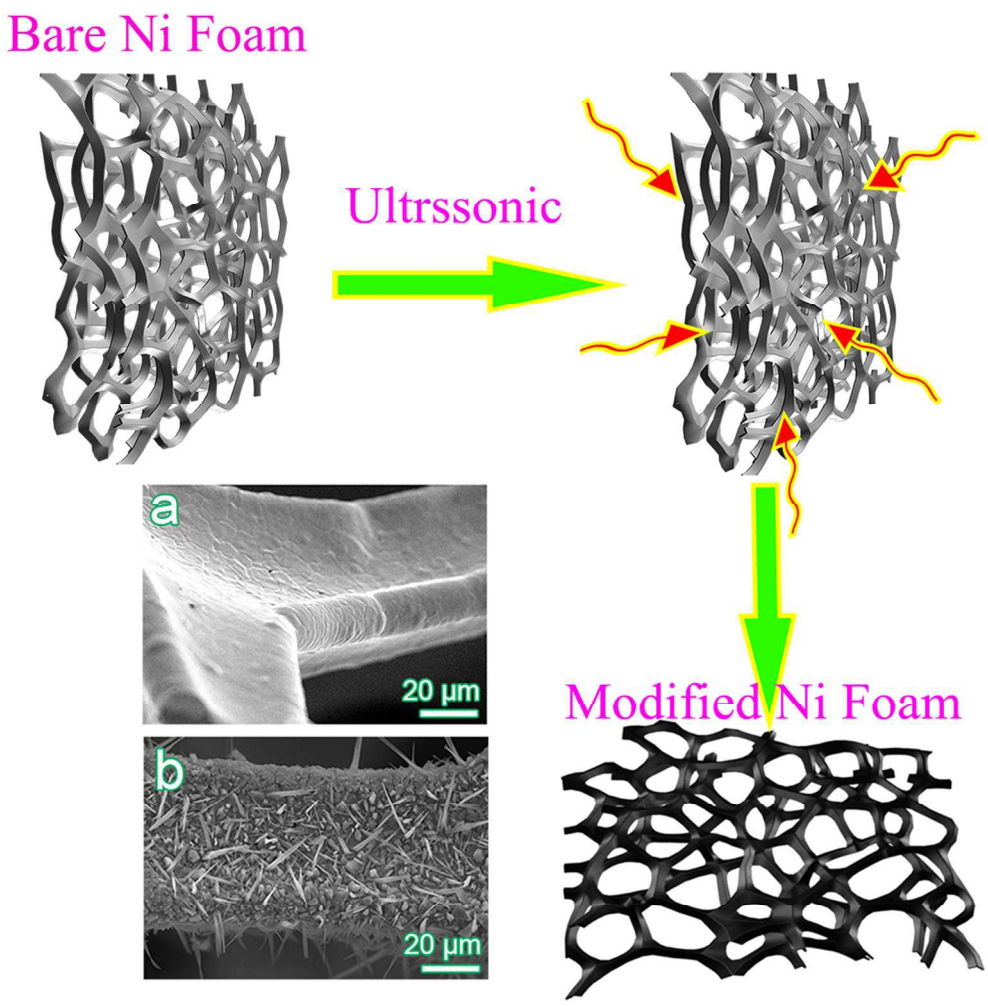

99x99mm (300 x 300 DPI)